DALTON FULL PAPER

Hydrothermal synthesis and structural characterization of organically templated zinc vanadium phosphates: [Zn(2,2′-bipyridine)(VO_2)(PO_4)], [Zn(2,2′:6′,2″-terpyridine)-(VO_2)(PO_4)], and [Zn(1,10-phenanthroline)(ZnVO)$(PO_4)_2$]

Robert C. Finn and Jon Zubieta *

Department of Chemistry, Syracuse University, Syracuse, NY 13244, USA

Received 20th April 2001, Accepted 7th December 2001
First published as an Advance Article on the web 8th February 2002

The hydrothermal reactions of zinc oxide, phosphoric acid, sodium orthovanadate, and the appropriate polyimine ligand at 200 °C for 95, 68, and 42.5 h, respectively, have yielded three novel compounds, [Zn(bpy)(VO_2)(PO_4)] (**1**), [Zn(terpy)(VO_2)(PO_4)] (**2**), and [Zn(*o*-phen)(ZnVO)$(PO_4)_2$] (**3**). Compounds **1** and **2** are both one-dimensional chains with discreet {$V_2P_2O_4$} rings linked through zinc organoimine components. Compound **3** exhibits unusual {$V_2P_4O_{18}$} subunits which are bound through fully bridging zinc tetrahedra to form a two-dimensional sheet. The sheet is further surface decorated by {Zn(*o*-phen)}$^{2+}$ moieties.

Introduction

The ability of an organic component to modify a metal oxide structure is now well documented.[1–4] The organic moiety may adopt a number of roles, such as chelator,[5] tethering agent,[6] charge-compensating cation,[7] or space-filling agent,[8] which has allowed for the development of new classes of organic–inorganic hybrid materials.

One successful approach in the design of such composite materials has utilized hydrothermal techniques. The hydrothermal temperature range of 100–250 °C allows retention of the structural integrity of the organic subunit, as well as overcoming solubility differences often encountered with mixed organic–inorganic starting materials. The hydrothermal regime affords metastable products, which include open framework materials, in which the organic subunit is incorporated into the inorganic oxide.[9,10] Although previously reported examples of zinc vanadium phosphate are dense phase materials,[11–13] our success in preparing open framework metal phosphates[14–16] under hydrothermal conditions encouraged us to investigate the zinc vanadium phosphate system more extensively.

Recent studies[3] of the zinc phosphate system with tetramine ligands under varying conditions produced eight unique structures, varying from one-dimensional chains to three-dimensional structures with elaborate channels. These structures provide important examples of the variety of polyhedral connectivities which evolve in the hydrothermal regime. Subtle manipulation of reaction conditions and judicious choice of the organic component can often lead to dramatic differences in products.[17–19]

As we have previously demonstrated,[20,21] a secondary metal–ligand subunit, such as a Zn(II)–organoimine moiety, may profoundly influence the structure of a vanadium phosphate. This allows considerable manipulation of the parent system through the coordination preferences of the secondary metal, ligation of the organic subunit, as well as spatial extension of the ligand. The introduction of zinc in a secondary metal–ligand subunit expands our ongoing investigations of first row transition elements in M′–vanadium oxide–phosphate–ligand systems, which were initiated with the copper series.[5,19–21] In this paper we discuss the synthesis and characterization of the one-dimensional materials [Zn(2,2′-bpy)(VO_2)(PO_4)] (**1**), and [Zn(terpy)(VO_2)(PO_4)] (**2**), and of the two-dimensional [Zn(*o*-phen)(ZnVO)$(PO_4)_2$] (**3**).

Discussion and results

[Zn(bpy)(VO_2)(PO_4)] (**1**) was synthesized hydrothermally through the reaction of ZnO, Na_3VO_4, 2,2′-bipyridine (bpy), H_3PO_4 (85%) and water in the molar ratio 5.14 : 1.52 : 1.00 : 7.59 : 1184 in a Parr acid digestion bomb. The mixture was stirred briefly and subsequently heated to 200 °C for 95 h. Upon cooling, the reaction gave clear colorless rhombic crystals suitable for X-ray diffraction in 60% yield. The synthesis of compound **1** suggested the modification of the ligand type in the preparation of [Zn(terpy)(VO_2)(PO_2)] (**2**). A reaction mixture of ZnO, 2,2′:6′,2″-terpyridine (terpy), Na_3VO_4, H_3PO_4 (85%) and H_2O in the molar ratio 3.75 : 1.00 : 2.58 : 15.21 : 2400 was stirred briefly and heated to 200 °C for 68 h to give clear colorless rods that were characterized through single crystal X-ray diffraction. Similarly, a reaction mixture of ZnO, Na_3VO_4, H_3PO_4 (85%), 1,10-phenanthroline, water and tetrabutylammonium hydroxide (40%) in the molar ratio 1.14 : 1.00 : 12.37 : 1.04 : 1100 : 2.50 was heated to 200 °C for 42.5 h, to give emerald green crystals of [(Zn(*o*-phen))(ZnVO)-$(PO_4)_2$] (**3**) in 65% yield. The infrared spectra of compounds **1**, **2**, and **3** revealed broad bands in the 900–970 cm^{-1} region attributed to *ν*(V=O), a series of bands in the 1100–1600 cm^{-1} range characteristic of *ν*(P–O), and peaks characteristic of *ν*(C–H, C–C, C–N) of the respective polyimine ligand throughout the spectra. Thermogravimetric analysis was performed on compounds **1**–**3**; revealing structures thermally stable up to *ca.* 400 °C in the case of **1** and **3**; however, **2** exhibited loss of ligand in three steps beginning at 273 °C.

[Zn(bpy)(VO_2)(PO_4)] (**1**) is a one-dimensional chain compound of discreet {$V_2P_2O_4$} cyclic units linked through corner-sharing {Zn(bpy)O_3} subunits. As seen in Fig. 1 (see also Table 1), each square pyramidal Zn(II) site completes its coordination sphere through two bpy nitrogen donors, one phosphate oxo-group and one vanadate bridging oxo-group in the basal plane, with the apical position defined by a phosphate oxygen bridging to an adjacent cyclic subunit. The cyclic motif itself is comprised of alternating {VO_4} and {PO_4} corner-sharing

 DOI: 10.1039/b103994f

Table 1 Bond lengths (Å) and angles (°) for [Zn(bpy)(VO_2)(PO_4)] (**1**)[a]

Zn(1)–O(2)	1.9456(16)	O(1)–Zn(1)–N(1)	95.74(7)
Zn(1)–O(1)	1.9844(15)	N(2)–Zn(1)–N(1)	78.41(7)
Zn(1)–N(2)	2.0730(19)	O(2)–Zn(1)–O(3)	90.92(6)
Zn(1)–N(1)	2.1046(18)	O(1)–Zn(1)–O(3)	88.95(6)
Zn(1)–O(3)	2.1819(15)	N(2)–Zn(1)–O(3)	88.26(7)
V(2)–O(6)	1.6081(16)	N(1)–Zn(1)–O(3)	162.52(7)
V(2)–O(3)	1.6463(16)	O(6)–V(2)–O(3)	108.46(8)
V(2)–O(4)	1.8497(15)	O(6)–V(2)–O(4)	108.39(8)
V(2)–O(5)	1.8505(16)	O(3)–V(2)–O(4)	111.05(7)
P(3)–O(2)#1	1.5046(16)	O(6)–V(2)–O(5)	111.35(8)
P(3)–O(1)	1.5275(16)	O(3)–V(2)–O(5)	109.18(8)
P(3)–O(5)#2	1.5577(16)	O(4)–V(2)–O(5)	108.43(7)
P(3)–O(4)	1.5896(16)	O(2)#1–P(3)–O(1)	114.38(9)
		O(2)#1–P(3)–O(5)#2	108.64(9)
O(2)–Zn(1)–O(1)	107.96(7)	O(1)–P(3)–O(5)#2	109.68(9)
O(2)–Zn(1)–N(2)	106.11(7)	O(2)#1–P(3)–O(4)	110.15(9)
O(1)–Zn(1)–N(2)	145.85(7)	O(1)–P(3)–O(4)	108.04(9)
O(2)–Zn(1)–N(1)	103.52(7)	O(5)#2–P(3)–O(4)	105.59(9)

[a] Symmetry transformations used to generate equivalent atoms: #1 $-x+1, -y+1, -z+2$; #2 $-x, -y+1, -z+1$.

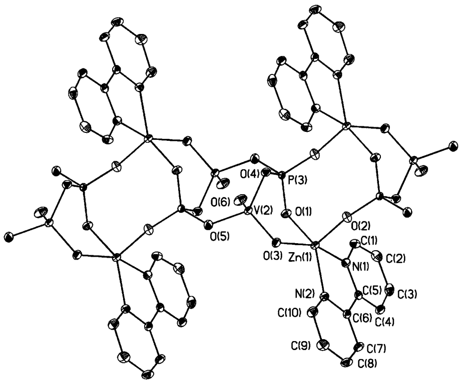

Fig. 1 The one-dimensional structure of [Zn(bpy)(VO_2)(PO_4)] (**1**), with 50% thermal ellipsoids and the atom-labeling scheme.

tetrahedra. Therefore, each phosphate tetrahedron is fully bridging: two oxo-groups to two adjacent vanadium sites, and two oxo-groups to two zinc sites. This bridging geometry generates a second, somewhat unusual, {$P_2Zn_2O_4$} eight-membered ring. Another consequence of the bridging {Zn(bpy)} subunit is the formation of a {$ZnVPO_3$} six-membered ring in a "boat" conformation.

We have previously observed dramatic structural consequences upon introducing ligands of increased steric demand. This, however, is not the case when comparing compound **1** to [Zn(terpy)(VO_2)(PO_4)] (**2**). The introduction of an additional pyridyl group to the ligand has only minor structural consequences. Thus, the {$V_2P_2O_4$} cyclic substructure of (**1**) is retained in the structure of (**2**). As shown in Fig. 2 (see also

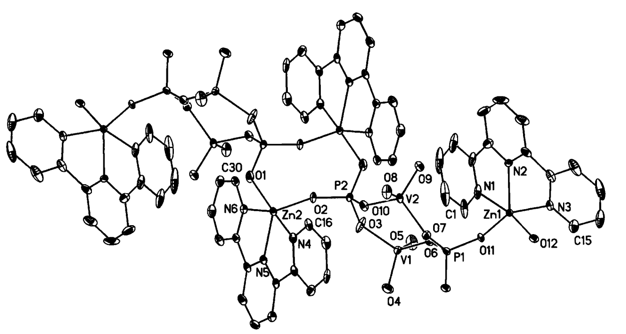

Fig. 2 The one-dimensional structure of [Zn(terpy)(VO_2)(PO_4)] (**2**), with 50% thermal ellipsoids and the atom-labeling scheme.

Table 2), the main structural difference between compounds **1** and **2** is the bridging mode of the secondary metal subunit between {$V_2P_2O_4$} rings. The zinc(II) square pyramidal site bonds to three nitrogens of the terpy ligand and one phosphate oxo-group in the basal plane, and completes the coordination with one bridging phosphate oxo-group in the apical position. This results in an expansion of the chain length by moving the {$V_2P_2O_4$} rings *ca.* 0.48 Å apart with respect to **1**, and also in less puckering within the ring itself. The coordination sphere about the phosphate tetrahedra is identical to that of compound **1**, both with respect to the bridging modes and bond lengths (1.557 and 1.554 Å, for **1** and **2**, respectively). The bonding at vanadium is affected by the increased denticity of the ligand, which allows the zinc site only two corner-sharing contacts with the {$V_2P_2O_4$} rings, rather than the three observed in compound **1**. The vanadate tetrahedra each bond to two bridging phosphate oxo-groups; however, the increased ligand bulk and denticity results in the absence of Zn–O–V bridging units, resulting in two terminal oxo-groups per vanadium site.

It is also instructive to compare the structure of [Zn(bpy)(VO_2)(PO_4)] (**1**) to that of the Cu(II) analogue, [Cu(bpy)(VO_2)(PO_4)],[22] which while a compositionally identical member of the [M(bpy)(VO_2)(PO_4)] type, exhibits a dramatically different structure. As shown in Fig. 3(a), [Cu(bpy)(VO_2)(PO_4)]

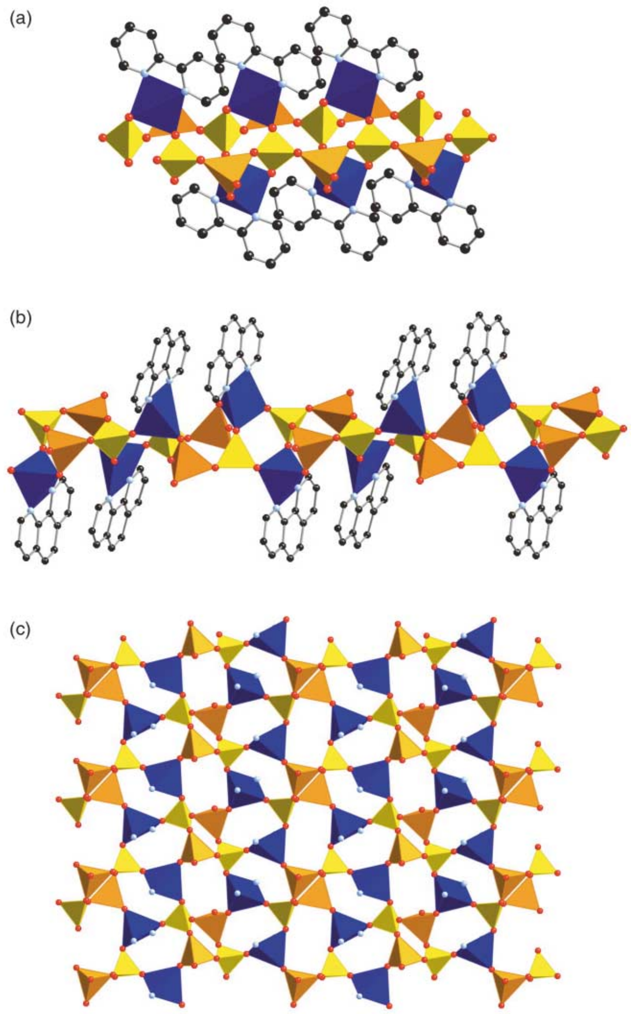

Fig. 3 Polyhedral representations of (a) the chain structure of [Cu(bpy)(VO_2)(PO_4)] (copper is shown as blue polyhedra), (b) the chain of [Cu(*o*-phen)(VO_2)(PO_4)], and (c) the metal oxide layer of the three-dimensional [Cu(4,4′-bpy)(VO_2)(PO_4)].

can be described as two infinite {(VO_2)(PO_4)} chains with {Cu(bpy)}$^{2+}$ subunits, both passivating the surface as well as connecting the two chains. In this case, the V/P/O subunit itself is one-dimensional and the secondary metal ligand subunit does not influence the overall dimensionality of the structure. Substitution of {Cu(*o*-phen)}$^{2+}$ for {Cu(bpy)}$^{2+}$ again leads to

Table 2 Bond lengths (Å) and angles (°) for $[Zn(tpy)(VO_2)(PO_4)]$ (**2**)[a]

Zn(1)–O(11)	1.965(2)	N(5)–Zn(2)–N(4)	76.30(11)
Zn(1)–O(12)	1.967(2)	O(1)–Zn(2)–N(6)	94.27(11)
Zn(1)–N(2)	2.097(3)	O(2)–Zn(2)–N(6)	94.98(10)
Zn(1)–N(1)	2.155(3)	N(5)–Zn(2)–N(6)	75.39(11)
Zn(1)–N(3)	2.182(3)	N(4)–Zn(2)–N(6)	151.04(11)
Zn(2)–O(1)	1.950(3)	O(5)–V(1)–O(4)	107.48(14)
Zn(2)–O(2)	1.953(2)	O(5)–V(1)–O(6)	108.93(12)
Zn(2)–N(5)	2.088(3)	O(4)–V(1)–O(6)	110.46(13)
Zn(2)–N(4)	2.158(3)	O(5)–V(1)–O(3)	110.18(15)
Zn(2)–N(6)	2.187(3)	O(4)–V(1)–O(3)	109.64(14)
V(1)–O(5)	1.619(3)	O(6)–V(1)–O(3)	110.11(11)
V(1)–O(4)	1.621(3)	O(8)–V(2)–O(9)	109.11(13)
V(1)–O(6)	1.871(2)	O(8)–V(2)–O(10)	107.80(12)
V(1)–O(3)	1.878(3)	O(9)–V(2)–O(10)	110.25(12)
V(2)–O(8)	1.624(2)	O(8)–V(2)–O(7)	108.40(13)
V(2)–O(9)	1.627(2)	O(9)–V(2)–O(7)	111.40(12)
V(2)–O(10)	1.848(2)	O(10)–V(2)–O(7)	109.79(11)
V(2)–O(7)	1.877(3)	O(5)–V(1)–O(4)	107.48(14)
P(1)–O(12)#1	1.522(3)	O(5)–V(1)–O(6)	108.93(12)
P(1)–O(11)	1.527(2)	O(4)–V(1)–O(6)	110.46(13)
P(1)–O(6)	1.564(3)	O(5)–V(1)–O(3)	110.18(15)
P(1)–O(7)	1.571(3)	O(4)–V(1)–O(3)	109.64(14)
P(2)–O(1)#2	1.517(3)	O(6)–V(1)–O(3)	110.11(11)
P(2)–O(2)	1.522(2)	O(8)–V(2)–O(9)	109.11(13)
P(2)–O(3)	1.554(3)	O(8)–V(2)–O(10)	107.80(12)
P(2)–O(10)	1.569(3)	O(9)–V(2)–O(10)	110.25(12)
		O(8)–V(2)–O(7)	108.40(13)
O(11)–Zn(1)–O(12)	115.90(10)	O(9)–V(2)–O(7)	111.40(12)
O(11)–Zn(1)–N(2)	111.08(11)	O(10)–V(2)–O(7)	109.79(11)
O(12)–Zn(1)–N(2)	132.97(10)	O(12)#1–P(1)–O(11)	113.12(14)
O(11)–Zn(1)–N(1)	105.67(10)	O(12)#1–P(1)–O(11)	113.12(14)
O(12)–Zn(1)–N(1)	93.36(12)	O(12)#1–P(1)–O(6)	109.87(13)
N(2)–Zn(1)–N(1)	75.44(13)	O(11)–P(1)–O(6)	108.41(14)
O(11)–Zn(1)–N(3)	97.75(10)	O(12)#1–P(1)–O(7)	108.59(14)
O(12)–Zn(1)–N(3)	96.50(11)	O(11)–P(1)–O(7)	110.59(13)
N(2)–Zn(1)–N(3)	75.13(12)	O(6)–P(1)–O(7)	106.01(14)
N(1)–Zn(1)–N(3)	147.40(12)	O(1)#2–P(2)–O(2)	113.46(15)
O(1)–Zn(2)–O(2)	114.54(11)	O(1)#2–P(2)–O(3)	110.53(17)
O(1)–Zn(2)–N(5)	135.11(11)	O(2)–P(2)–O(3)	111.12(14)
O(2)–Zn(2)–N(5)	109.88(11)	O(1)#2–P(2)–O(10)	109.22(14)
O(1)–Zn(2)–N(4)	101.48(12)	O(2)–P(2)–O(10)	106.78(13)
O(2)–Zn(2)–N(4)	100.23(10)	O(3)–P(2)–O(10)	105.33(15)

[a] Symmetry transformations used to generate equivalent atoms: #1 $-x + 1, -y + 1, -z + 2$; #2 $-x, -y, -z + 1$.

a one-dimensional chain in $[Cu(o\text{-phen})(VO_2)(PO_4)]$,[22,23] shown in Fig. 3(b). This chain is nearly identical to that of $[Zn(bpy)(VO_2)(PO_4)]$ (**1**) with the $\{V_2P_2O_4\}$ cyclic units apparent. The coordination geometry of Cu(II) in $[Cu(o\text{-phen})(VO_2)(PO_4)]$ is completed by two nitrogens of the *o*-phen ligand and two phosphate oxo-groups from two different clusters in the basal plane, with a vanadium oxo-group occupying the apical position. The only difference between compound **1** and the {Cu(*o*-phen)} analogue is the relative siting of donor groups about the metal polyhedra: in the zinc(II) case, the apical position is occupied by a phosphate oxo-group and the basal plane is defined by one phosphate oxo-group, one vanadate oxo-group, and two nitrogens from the ligand. This subtle difference in bonding mode allows for a more close-packed chain in $[Cu(o\text{-phen})(VO_2)(PO_4)]$ in comparison to **1**.

While the structure of **1**, **2**, $[Cu(bpy)(VO_2)(PO_4)]$, and $[Cu(o\text{-phen})(VO_2)(PO_4)]$ may reflect the different coordination preferences of Zn(II) and Cu(II), ligand geometry may also profoundly influence the structure. For example, in contrast to the one-dimensional structure of $[Cu(2,2'\text{-bpy})(VO_2)(PO_4)]$, the structure of the analogous material with a linear dipodal ligand, $[Cu(4,4'\text{-bpy})(VO_2)(PO_4)]$, is three-dimensional.[22] As shown in Fig. 3(c), the geometry of the tethering ligand allows bridging of the $\{Cu(VO_2)(PO_4)\}$ layers to produce the characteristic structure type of alternating inorganic layers and organic domains. It is noteworthy that the $\{P_2V_2O_4\}$ cyclic structure is again observed, although in this case, in conjunction with $\{Cu_2V_2P_2O_6\}$ and $\{Cu_2VP_2O_5\}$ rings.

The structure of $[Zn(o\text{-phen})(ZnVO)(PO_4)_2]$ (**3**) is somewhat curious and unanticipated. The network structure of **3** is shown in Fig. 4(a) (see also Table 3). While a $\{V_2P_2O_4\}$ ring substructure is evident, there are a number of unusual features associated with this unit in **3**, when compared to those formed in **1**, **2**, and $[Cu(4,4'\text{-bpy})(VO_2)(PO_4)]$. As shown in Fig. 4(b), the vanadium sites are square pyramidal rather than tetrahedral and, furthermore, the vanadium polyhedra engage in an edge-sharing interaction with an exocyclic phosphate group. This unusual polyhedral connectivity results in the embedded cluster motif $\{V_2P_4O_{18}\}$. The phosphate tetrahedra of the $\{V_2P_2O_4\}$ ring engage in corner-sharing to two vanadium sites of the ring and to a tetrahedral $\{ZnO_4\}$ site, and in a triply-bridging interaction with a $\{ZnO_4\}$ site and a $\{Zn(o\text{-phen})O_3\}$ site. The square pyramidal vanadium(IV) center exhibits two oxo-groups bridging to phosphates of the ring, an oxo-group linking the exocyclic phosphate and a $\{ZnO_4\}$ site, and an oxo-group bridging to the exocyclic phosphate and a $\{Zn(o\text{-phen})O_3\}$ square pyramid in the basal plane; the apical position is defined by a terminal oxo-group. Valence bond calculations, as well as the green color of the crystals confirm that the vanadium is present in the +4 oxidation state, rather than the fully oxidized +5 observed for **1** and **2**.

A noteworthy feature of the structure of **3** is the presence of two distinct Zn(II) geometries; one is a tetrahedral $\{ZnO_4\}$ center which bridges three $\{V_2P_4O_{18}\}$ clusters and one $\{Zn(o\text{-phen})O_3\}$ site. Two of the oxygen atoms bridge to phosphorus centers of adjacent clusters; one is triply-bridging to a vanadium site and a phosphorus of a cluster; and the fourth oxygen atom bridges to a phosphorus of a third cluster and to a

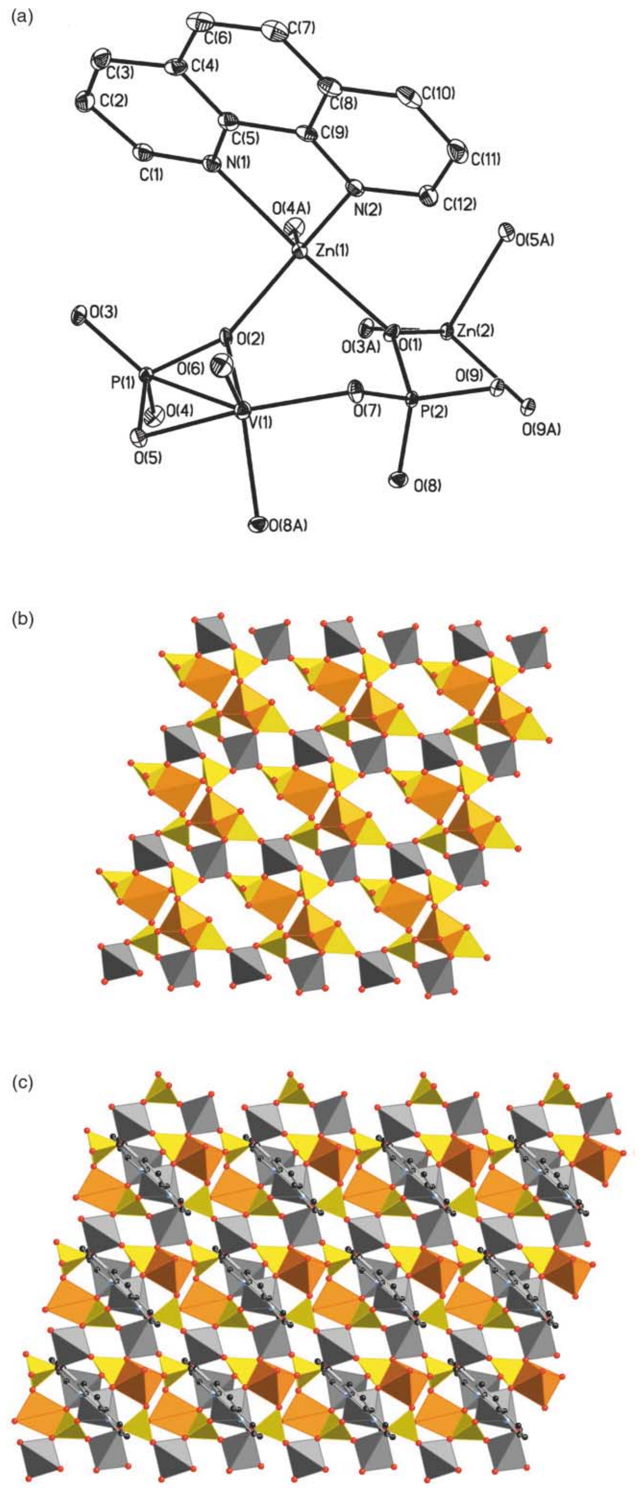

Fig. 4 (a) A view of the structure of $[Zn(o\text{-phen})(ZnVO)(PO_4)_2]$ (**3**), with 50% thermal ellipsoids and the atom-labeling scheme. (b) A polyhedral representation of the $\{(ZnVO)(PO_4)_2\}$ network structure of $[Zn(o\text{-phen})(ZnVO)(PO_4)_2]$ (**3**), omitting the $\{Zn(o\text{-phen})\}^{2+}$ subunits which decorate the faces of the layer. Zinc is represented in gray, vanadium in orange, phosphate in yellow, oxygen in red spheres, nitrogen in light blue spheres and carbon in black. (c) The overall structure of compound **3**, showing the metal–ligand subunit occupying the cavities within the layer.

$\{Zn(o\text{-phen})O_3\}$ subunit. The square pyramidal Zn(II) center coordinates to two nitrogen donors of the *o*-phen ligand, one bridging phosphate oxo-group of one cluster, and one triply-bridging phosphate oxo-group, to a second cluster and to a zinc tetrahedron, in the basal plane; the apical position is occupied by a triply-bridging vanadium phosphate oxo-group of the second cluster.

The $\{Zn(o\text{-phen})\}^{2+}$ metal–ligand subunits decorate the surfaces of the $\{Zn(VO)(PO_4)_2\}_n^{2n-}$ oxide layer, shown in Fig. 4(c), and span the 3.4 Å × 6.3 Å intralamellar cavities of this network. The organic groups project into the interlamellar void.

Conclusions

The title compounds, as well as the examples in Fig. 3, demonstrate the inherent structural diversity in the hydrothermal regime. However, the propensity of vanadium phosphates to form the $\{V_2P_2O_{12}\}$ tetranuclear unit in this system provides some insight into building block preferences within this chemistry. The ability of the metal oxide to adopt a confirmation which will accept the secondary metal ligand subunit within the structure allows for the formation of a vast number of organic–inorganic hybrid materials.

Transition metal phosphates continue to attract attention as lamellar and open framework materials potentially manifesting porous properties.[24–26] The search for new materials of this family has now focused on structural modification and design of oxovanadium phosphates through the introduction of organic components as charge-compensating, space-filling and overall structure-directing cations. One approach has been to introduce a secondary metal–ligand subunit as a covalent attachment to the oxovanadium phosphate substructure. This strategy has produced a variety of novel structural types by exploiting the hydrothermal domain as a solubilization and recrystallization medium. Further development of synthetic design strategies appears inherent in the systematic variation of the secondary metal and its coordination preferences, the geometry and ligation of the organic moiety, and the overall reaction conditions.

Experimental

All reagents were obtained from Aldrich Chemical Co. and used without further purification. Syntheses were carried out in 23 ml polytetrafluoroethylene-lined stainless steel containers under autogenous pressure. Distilled water was purified to below 3.0 Ω in-house with a Barnstead Model 525 Biopure system.

Synthesis

$[Zn(bpy)(VO_2)(PO_4)]$ (1). A solution of ZnO (0.198 g, 2.43 mmol), Na_3VO_4 (0.132 g, 0.718 mmol), 2,2′-dipyridyl (0.073 g, 0.473 mmol), H_3PO_4 (85%) (0.352 g, 3.59 mmol), and H_2O (10.10 g, 560 mmol) in the molar ratio 5.14 : 1.52 : 1.00 7.59 : 1184 was heated to 200 °C for 95 h. After cooling to room temperature, clear colorless crystals of $[Zn(bpy)(VO_2)(PO_4)]$ were isolated in 60% yield. IR (KBr pellet, cm^{-1}): 1597(sh), 1542(s), 1508(s), 1474(sh), 1442(sh), 1313(m), 1188(m), 1061(m), 1026(m), 969(br) 907(m).

$[Zn(terpy)(VO_2)(PO_4)]_2$ (2). A solution of ZnO (0.073 g, 0.90 mmol), terpyridine (0.056 g, 0.24 mmol), Na_3VO_4 (0.114 g, 0.62 mmol), H_3PO_4 (85%) (0.358 g, 3.65 mmol), and H_2O (10.43 g, 578 mmol) in the molar ratio 3.75 : 1.00 : 2.58 : 15.21 : 2400 was heated to 200 °C for 68 h. After cooling to room temperature, clear colorless rods of $[Zn(terpy)(VO_2)(PO_4)]$ were isolated in 60% yield. IR (KBr pellet, cm^{-1}): 1597(sh), 1578(sh), 1477(m), 1452(m), 1322(br), 1253(s), 1072(br), 976(m), 778(sh).

$[Zn(o\text{-phen})(ZnVO)(PO_4)_2]$ (3). A solution of ZnO (0.049 g, 0.602 mmol), Na_3VO_4 (0.097 g, 0.527 mmol), H_3PO_4 (85%) (0.639 g, 6.52 mmol), phenanthroline (0.099 g, 0.549 mmol), H_2O (10.44 g, 579 mmol), and tetrabutylammonium hydroxide (40%; 0.343 g, 1.32 mmol) in the molar ratio 1.14 : 1.00 : 12.37 : 1.04 : 1100 : 2.50 was heated to 200 °C for 42.5 h. After cooling

Table 3 Bond lengths (Å) and angles (°) for $[Zn(o\text{-phen})(ZnVO)(PO_4)_2]$ (**3**)[a]

Zn(1)–O(4)#1	1.943(2)	O(3)#1–Zn(2)–O(1)	105.26(9)
Zn(1)–O(2)	2.034(2)	O(9)#2–Zn(2)–O(5)#3	101.29(9)
Zn(1)–N(2)	2.081(3)	O(3)#1–Zn(2)–O(5)#3	105.95(9)
Zn(1)–O(1)	2.108(2)	O(1)–Zn(2)–O(5)#3	110.19(9)
Zn(1)–N(1)	2.138(3)	O(6)–V(1)–O(7)	103.76(11)
Zn(2)–O(9)#2	1.905(2)	O(6)–V(1)–O(8)#4	109.11(11)
Zn(2)–O(3)#1	1.930(2)	O(7)–V(1)–O(8)#4	92.77(9)
Zn(2)–O(1)	1.967(2)	O(6)–V(1)–O(5)	106.81(10)
Zn(2)–O(5)#3	1.986(2)	O(7)–V(1)–O(5)	146.97(9)
V(1)–O(6)	1.598(2)	O(8)#4–V(1)–O(5)	88.89(9)
V(1)–O(7)	1.939(2)	O(6)–V(1)–O(2)	110.82(11)
V(1)–O(8)#4	1.950(2)	O(7)–V(1)–O(2)	87.03(9)
V(1)–O(5)	2.018(2)	O(8)#4–V(1)–O(2)	138.90(9)
V(1)–O(2)	2.022(2)	O(5)–V(1)–O(2)	70.71(8)
V(1)–P(1)	2.6970(9)	O(6)–V(1)–P(1)	114.59(9)
P(1)–O(4)	1.504(2)	O(7)–V(1)–P(1)	118.15(7)
P(1)–O(3)	1.511(2)	O(8)#4–V(1)–P(1)	115.91(7)
P(1)–O(2)	1.570(2)	O(5)–V(1)–P(1)	35.42(6)
P(1)–O(5)	1.573(2)	O(2)–V(1)–P(1)	35.33(6)
P(2)–O(9)	1.526(2)	O(4)–P(1)–O(3)	113.58(12)
P(2)–O(7)	1.533(2)	O(4)–P(1)–O(2)	112.21(12)
P(2)–O(8)	1.542(2)	O(3)–P(1)–O(2)	111.54(12)
P(2)–O(1)	1.563(2)	O(4)–P(1)–O(5)	110.82(12)
		O(3)–P(1)–O(5)	111.34(12)
O(4)#1–Zn(1)–O(2)	116.20(9)	O(2)–P(1)–O(5)	96.07(11)
O(4)#1–Zn(1)–N(2)	130.06(10)	O(4)–P(1)–V(1)	121.21(9)
O(2)–Zn(1)–N(2)	112.84(9)	O(3)–P(1)–V(1)	125.20(9)
O(4)#1–Zn(1)–O(1)	94.32(8)	O(2)–P(1)–V(1)	48.13(8)
O(2)–Zn(1)–O(1)	90.65(8)	O(5)–P(1)–V(1)	48.01(8)
N(2)–Zn(1)–O(1)	93.99(9)	O(9)–P(2)–O(7)	109.27(12)
O(4)#1–Zn(1)–N(1)	91.93(9)	O(9)–P(2)–O(8)	112.96(12)
O(2)–Zn(1)–N(1)	89.94(9)	O(7)–P(2)–O(8)	110.32(12)
N(2)–Zn(1)–N(1)	79.09(10)	O(9)–P(2)–O(1)	108.60(12)
O(1)–Zn(1)–N(1)	172.71(9)	O(7)–P(2)–O(1)	108.56(12)
O(9)#2–Zn(2)–O(3)#1	119.47(9)	O(8)–P(2)–O(1)	106.99(12)
O(9)#2–Zn(2)–O(1)	114.21(9)		

[a] Symmetry transformations used to generate equivalent atoms: #1 $-x + 2, -y + 2, -z$; #2 $-x + 3, -y + 1, -z$; #3 $x + 1, y, z$; #4 $-x + 2, -y + 1, -z$; #5 $x - 1, y, z$.

Table 4 Summary of crystal data and structure refinement for **1**–**3**

Compound	$[Zn(bpy)(VO_2)(PO_4)]$	$[Zn(tpy)(VO_2)(PO_4)]$	$[Zn(o\text{-phen})(ZnVO)(PO_4)_2]$
Empirical formula	$C_{10}H_8N_2O_6PVZn$	$C_{15}H_{11}N_3O_6PVZn$	$C_{12}H_8N_2O_9P_2VZn_2$
Formula weight	399.47	476.55	567.82
Crystal size/mm	0.24 × 0.16 × 0.07	0.31 × 0.12 × 0.04	0.28 × 0.27 × 0.24
Crystal system	Monoclinic	Triclinic	Triclinic
Space group	$P2_1/c$	$P\bar{1}$	$P\bar{1}$
a/Å	7.7860(3)	10.4536(2)	7.9657(3)
b/Å	17.2896(7)	11.8867(2)	9.0824(4)
c/Å	9.7897(4)	13.9981(1)	11.8322(5)
α/°	90	93.0340(1)	81.421(1)
β/°	104.744(1)	93.766(1)	71.301(1)
γ/°	90	105.468(1)	74.998(1)
Volume/Å^3	1274.4(1)	1668.27(4)	781.16(6)
Z	4	2	2
D_{calc}/g cm^{-3}	2.082	1.897	2.414
F(000)	396	476	558
λ/Å	0.71073	0.71073	0.71073
μ/mm^{-1}	2.770	2.135	2.414
Unique data	3059	7245	3633
Final R indices, $R1$ ($wR2$)	0.0340 (0.0645)	0.0621 (0.0966)	0.0363 (0.0897)

to room temperature, green crystals of $[Zn(o\text{-phen})(ZnVO)(PO_4)_2]_2$ were isolated in 65% yield. IR (KBr pellet, cm^{-1}): 1584(s), 1542(s), 1432(sh), 1182(sh), 1019(br), 1003(sh), 973(m), 950(m), 925(sh), 726(m).

X-Ray crystallography

Crystallographic data (Table 4) were collected with a Siemens P4 diffractometer equipped with a SMART CCD 1K system[27] using Mo-Kα radiation (λ = 0.71073 Å). The data were collected at 90(3) K and corrected for Lorentz and polarization effects. Absorption corrections were made using SADABS.[28] The structure solution and refinement were carried out using the SHELXL97[29] software package. The structures were solved using direct methods and all of the non-hydrogen atoms were located from the initial solution. After locating all of the non-hydrogen atoms in each structure, the model was refined against F^2, initially using isotropic, and later anisotropic, thermal displacement parameters, until the final value of Δ/σ_{max} was less than 0.001.

CCDC reference numbers 175194–175196.

See http://www.rsc.org/suppdata/dt/b1/b103994f/ for crystallographic data in CIF or other electronic format.

Acknowledgements

Thermogravimetric analysis was preformed by R. L. LaDuca, Jr. at King's College, Wilkes-Barre, PA. This work was supported by NSF grant CHE9987471.

References

1 A. K. Cheetham, G. Férey and T. Loiseau, *Angew. Chem., Int. Ed.*, 1999, **38**, 2638.
2 C. Livage, C. Egger and G. Férey, *Chem. Mater.*, 2000, **13**, 410 and references therein.
3 A. Choudhary, S. Natarajan and C. N. R. Rao, *Inorg. Chem.*, 2000, **39**, 4295.
4 P. Feng, X. Bu and G. D. Stucky, *Nature*, 1997, **388**, 735.
5 R. C. Finn and J. Zubieta, *J. Chem. Soc., Dalton Trans.*, 2000, 1821.
6 P. Braunstein, H.-P. Kormann, W. Meyer-Zaika, R. Pugin and G. Schmid, *Chem. Eur. J.*, 2000, **6**, 4637.
7 V. Soghomonian, Q. Chen, R. C. Haushalter, J. Zubieta, C. J. O'Connor and Y. S. Lee, *Chem. Mater.*, 1993, **5**, 1690.
8 G. Bonavia, R. C. Haushalter and J. Zubieta, *J. Solid State Chem.*, 1996, **126**(2), 292.
9 D. R. Corbin, J. F. Whitney, W. C. Fultz, G. D. Stucky, M. M. Eddy and A. K. Cheetham, *Inorg. Chem.*, 1986, **25**, 2279.
10 W. T. A. Harrison, M. L. F. Phillips, W. Clegg and S. J. Teat, *J. Solid State Chem.*, 1999, **148**, 433.
11 K. L. Idler and C. Calvo, *Can. J. Chem.*, 1975, **53**, 3665.
12 K. H. Lii and H. J. Tsai, *J. Solid State Chem.*, 1991, **90**, 291.
13 S. Boudin, A. Grandin, A. Leclaire, M. M. Borel and B. Raveau, *J. Solid State Chem.*, 1995, **115**, 140.
14 S. Ayyappan, G. Diaz de Delgado, A. K. Cheetham, G. Férey and C. N. R. Rao, *J. Chem. Soc., Dalton Trans.*, 1999, 2905.
15 S. Neeraj, S. Natarajan and C. N. R. Rao, *Chem. Mater.*, 1999, **11**, 1390.
16 W. T. A. Harrison, Z. Bircsak, L. Hannooman and Z. Zhang, *J. Solid State Chem.*, 1999, **147**, 154.
17 J. R. D. DeBord, Y. Zhang, R. C. Haushalter, J. Zubieta and C. J. O'Connor, *J. Solid State Chem.*, 1996, **122**, 251.
18 L.-M. Zheng, J.-S. Zhao, K.-H. Lii, L.-Y. Zhang, Y. Liu and X.-Q. Xin, *J. Chem. Soc., Dalton Trans.*, 1999, 939.
19 D. Hagrman, P. J. Hagrman and J. Zubieta, *Comments Inorg. Chem.*, 1999, **21**, 225.
20 R. Finn and J. Zubieta, *Chem. Commun.*, 2000, 1321.
21 R. C. Finn and J. Zubieta, *J. Chem. Soc., Dalton Trans.*, 2000, 1821.
22 Z. Shi, S. Feng, L. Zhang, G. Yang and J. Hua, *Chem. Mater.*, 2000, **12**, 2930.
23 R. C. Finn and J. Zubieta, *J. Phys. Chem. Solids*, 2001, **62**, 1513.
24 C. N. R. Rao, S. Natarajan and S. Neeraj, *J. Am. Chem. Soc.*, 2000, **122**, 2810 and references therein.
25 S. Natarajan, S. Neeraj, A. Choudhury and C. N. R. Rao, *Inorg. Chem.*, 2000, **39**, 142.
26 K.-H. Lii, Y.-F. Huang, V. Zima, C.-Y. Huang, H.-M. Lin, Y.-C. Jiang, F.-L. Liao and S.-L. Wang, *Chem. Mater.*, 1998, **10**, 2599 and references therein.
27 Siemens "Smart" Software Reference Manual, Siemens Analytical X-Ray Instruments, Inc., Madison, WI, 1994.
28 G. M. Sheldrick, SADABS, Program for Empirical Absorption Corrections, University of Göttingen, Germany, 1996.
29 G. M. Sheldrick, SHELXL97, Program for the Refinement of Crystal Structures, University of Göttingen, Germany, 1997.